2026 IEEE International Conference on Robotics and Automation (ICRA 2026)
June 1-5, 2026. Vienna, Austria

Soft robots grow a spine: Origami-inspired folding endoskeletal support for motion and stiffness control of inflatable robots

Junil Min[1], Matthew Robertson[2]

***Abstract*— We present a deployable inflatable robotic torso with an origami-inspired spine, designed to combine the inherent compliance of soft robots with the controllability of skeletal structures. Unlike simple inflatable cylinders, which deform unpredictably through membrane buckling, our approach embeds a foldable spine that defines discrete bending axes and enables repeatable motion. Pneumatic inflation provides compact self-deployment, external stiffening, and a compliant outer shell that serves as a protective contact interface, while tendon actuation delivers precise, joint-level control. Experiments demonstrate that the torso replicates and in some cases exceeds human spinal range of motion, and that combined tendon–pneumatic actuation doubles lateral stiffness compared to pneumatics alone. We further characterize stiffness–motion trade-offs across pressures, showing tunable performance relevant to contact-rich operation. This integration of origami endoskeletons with inflatable bodies advances deployable humanoid-scale robots, addressing the gap between compliant contact behavior and controlled movement.**

I. INTRODUCTION

Soft robotics provides inherently safe, compliant mechanisms for human–robot interaction across rehabilitation, wearable assistance, and surgical manipulation [1]–[9]. Yet extending soft principles to humanoid-scale systems that function in everyday settings remains difficult. A key limitation is that simple inflatable bodies deform primarily through *membrane buckling* rather than around well-defined bending axes; as a result, they exhibit uncontrolled curvature, hysteresis, and poor repeatability under load. To move beyond balloon-like compliance, humanoid soft robots need *internal structures* that define discrete degrees of freedom (DoFs) while preserving a compliant outer interface.

Portability and deployability are also critical for operation in constrained or remote environments (space, disaster response, field logistics), where compact, low-mass hardware is essential [10]–[13]. Prior efforts introduced deployable structures with passive stiffening [14] and inflatable arms for aerospace tasks [15], highlighting benefits in cost and stowage. Related systems have embedded skeletal components within soft or inflatable bodies to improve controllability at the limb/manipulator scale [16]–[18], but torso-level deployment with safe encapsulation and discrete joint control remains underexplored.

Deployability is not unique to origami: scissor-type deployable mechanisms and modular deployable truss structures have been widely studied for compact storage and large expansion ratios [11], [19]. These rigid-link systems typically deploy through jointed linkages and multi-member assemblies, sometimes using sliding elements [11], [19]. In contrast, origami-inspired mechanisms encode kinematic constraints directly within crease patterns in planar laminates, allowing folding to occur along designed crease lines without discrete mechanical hinges [20], [21]. This supports compact folding while still defining discrete bending axes within a continuous structure.

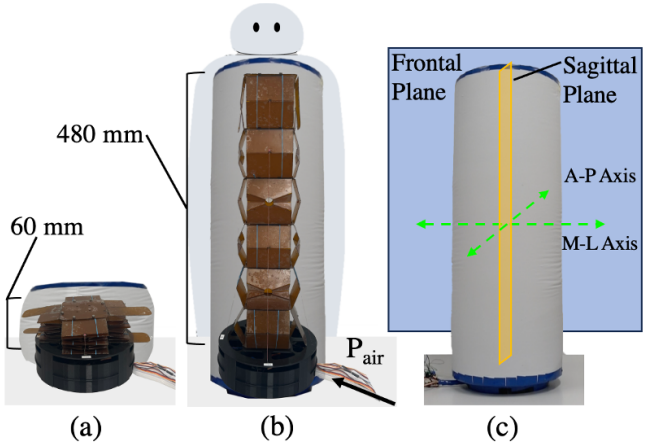

Fig. 1. (a) Collapsed torso (60 mm height). (b) Inflated torso (480 mm) with conceptual humanoid integration. (c) Fully deployed torso demonstrating sagittal and frontal plane motions.

Compared to limbs, manipulators, or modular devices that have been the primary focus of deployable and origami-inspired designs, the torso introduces a different set of system-level requirements. It typically houses much of a robot's internal hardware, serves as the central structural support for multiple appendages, and directly governs whole-body posture and balance. As such, the torso should not be treated as a static frame, but as a functional, active subsystem whose design impacts stability, safety, and adaptability. A compact or deployable arm, for instance, offers limited benefit if the torso remains a rigid and bulky core. Exploring torso deployability and stiffness modulation therefore addresses a critical but often overlooked component in humanoid robot design, and complements existing work on soft and inflatable technologies that has largely focused on extremities.

Origami-inspired mechanisms have been widely studied for their compactness, portability, and scalability, particularly in the design of limbs and modular devices. In contrast, applying these principles to the torso introduces different challenges and opportunities, since the torso is

[1] Department of Mechanical Engineering, Carnegie Mellon University, Pittsburgh, PA, USA.
[2] Department of Mechanical and Materials Engineering, Queen's University, Kingston, ON, Canada.

both a load-bearing structure and a central body segment that supports appendages and governs posture. Pneumagami modules leverage waterbomb folds for high-DoF pneumatic actuation [20], while self-locking folds enable tendon-driven stiffening with minimal hardware [21]. Origami concepts have also been demonstrated for amphibious locomotion [22] and interactive or assistive contexts [23]–[25]. In this work, we use the term *torso-scale* not only to indicate physical size, but also to emphasize the morphological and functional role of the torso as the robot's central body segment.

Inflatable systems complement origami by providing human-scale, inherently compliant shells. Recent examples include untethered isoperimetric robots [26] and blower-powered inflatable joints actuated by tendons [27]. However, bare inflatables struggle with strength and precise control due to excessive compliance and effectively infinite DoFs; simple inflatable cylinders bend only after local collapse, which is not repeatable or controllable under varying load.

Tendon-driven systems (TDS) enable precise, repeatable actuation with off-board actuators [28]–[30]. They have been integrated with variable-stiffness elements [29], elastomeric bodies [30], and origami chambers [31]–[34]. Parallel work has explored embedded skeletons in soft structures to reconcile strength with compliance [18]. Nevertheless, many hybrids rely on exposed rigid components that raise entanglement and safety concerns for close human interaction, or they target limb-scale devices rather than humanoid torsos [16], [17].

Humanoid-scale soft robot torsos also emphasize compliance and impact tolerance. Baloo is a large-scale hybrid soft-rigid robotic torso that uses pneumatic actuation for whole-arm manipulation and contact-rich interaction [35]. Similarly, GrowHR is a soft humanoid platform with growable bone-mimetic linkages that enables dynamic shape adaptation and safe human interaction [36]. At the system level, Lin *et al.* propose a variable-stiffness mechanism for wheeled humanoid robots to transition between compliant buffering and rigid support for anti-falling [37]. While these approaches address whole-body compliance, load capacity, or fall prevention, they do not focus on a deployable torso architecture that embeds discrete bending axes within a protective inflatable shell to achieve repeatable, joint-level control at humanoid scale.

We introduce a *deployable inflatable robotic torso* that integrates a foldable origami endoskeletal spine within a soft inflatable shell (Fig. 1). The inflatable body provides compact self-deployment, external stiffening, and a protective barrier that encapsulates complexity to reduce hard-contact exposure; the origami spine defines *discrete bending axes*, removing reliance on uncontrolled membrane buckling to determine motion; and tendon actuation yields *repeatable, joint-level control* with well-defined DoFs [38]. In contrast to prior tendon–pneumatic hybrids and inflatable manipulators [17], [27], [33], our contribution is a *torso-scale* integration that (i) enables stow-and-deploy operation, (ii) maintains a compliant encapsulation without exposed rigid elements, and (iii) empirically characterizes the stiffness–range-of-motion trade-off across pressures for task-tunable performance.

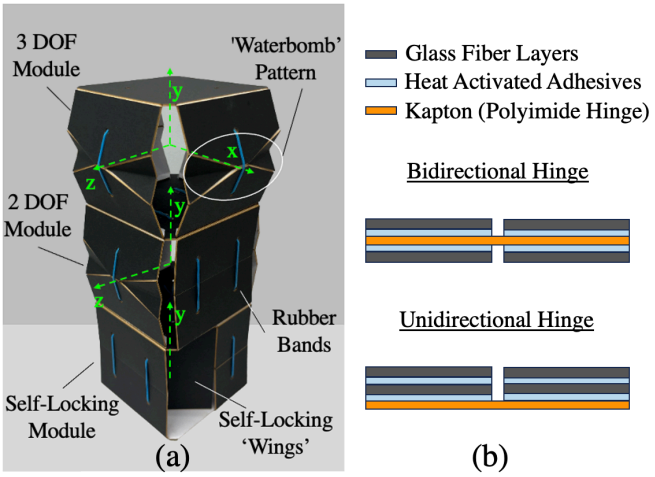

Fig. 2. (a) Origami spine with self-locking, 2-DoF, and 3-DoF modules. (b) Bidirectional vs. unidirectional Kapton–glass fiber hinge construction.

Beyond its mechanical design, a deployable torso with tunable stiffness has direct implications for several application domains. In humanoid robots, an inflatable exterior offers inherent contact compliance during physical interaction, while adjustable stiffness allows the torso to shift between compliant motion for contact and stable support for load-bearing. The compact stowage ratio (12.5% of deployed height) further makes the design relevant for deployable field systems that must be transported efficiently and deployed rapidly in unstructured environments, as well as wearable assistive devices where lightweight, adjustable support is critical.

The main contributions are:

- A humanoid-scale, self-deployable torso that embeds an origami spine within an inflatable shell to combine portability, compliance-focused encapsulation, and controllability.
- A dual-actuation strategy in which pneumatic inflation provides deployment and external stiffening, while tendons deliver discrete, repeatable joint control.
- An empirical characterization of stiffness–motion trade-offs versus pressure, showing tunable performance suitable for contact-rich operation.

II. Design

The inflatable robotic torso integrates three key elements: (i) modular origami-inspired spine segments, (ii) tendon-driven actuation for bending and joint control, and (iii) a pneumatically inflated shell that provides deployment, stiffening, and a protective interface (Fig. 1). Together, these create a hybrid system that is compact, compliance-focused, and controllable.

A. Spine Modules

The spine is composed of three origami module types (Fig. 2a): a self-locking module, a 2-DoF waterbomb-based module, and a 3-DoF spherical-like module. Each module

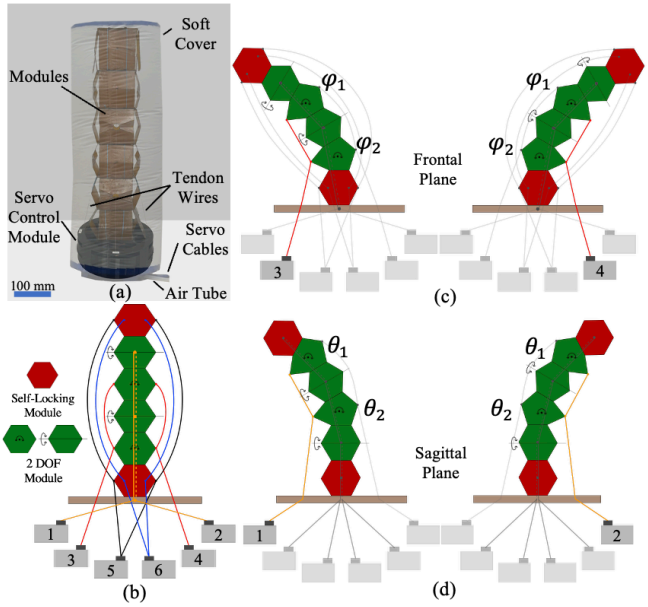

Fig. 3. (a) Torso with tendon routing and control base. (b) Spine module configuration. (c–d) Tendon-driven bending in frontal and sagittal planes.

consists of two rigid plates connected by foldable linkages, with rubber bands providing restoring force for deployment from the collapsed state. Each module has a height of approximately 80 mm, which establishes the scale of the torso and provides a reference for interpreting experimental displacements.

- **Self-locking:** Inspired by perpendicular folding [21], this module restricts motion to a single axis. Winged linkages can engage to lock the module, or disengage to allow folding. This provides precise control of stiffness and one DoF bending.
- **2-DoF:** Waterbomb-based fold enabling lateral bending and vertical-axis rotation [20].
- **3-DoF:** Extended waterbomb concept providing spherical-like mobility, positioned at the upper end of the spine for neck-like flexibility.

This modularity enables spine configurations with different ranges of motion (RoM) and stiffness profiles, allowing the same underlying architecture to be tuned for task-specific requirements.

B. Living Hinges

Modules incorporate Kapton–glass fiber laminate hinges (Fig. 2b). Two variants were fabricated:

- **Bidirectional:** Bends in both directions.
- **Unidirectional:** Provides passive stiffness in one direction while locking the other.

Hinges were heat-pressed at 140°C, 4000 lb force, for 75 s to ensure bonding. This localized the bending axes, maintained compactness, and improved repeatability across cycles. Kapton was chosen for its high fatigue resistance, thermal stability, and flexibility, while glass fiber constrains out-of-plane deformation and provides structural reinforcement in non-bending regions. Together, these materials achieve a balance between durability and low thickness, making the hinges lightweight while withstanding repeated actuation.

In practice, hinge design directly impacts mechanical reliability and limits undesired motion. Bidirectional hinges afford flexibility but may introduce unwanted compliance, while unidirectional hinges restrict back-bending in sensitive regions. By mixing both hinge types, the torso achieves human-like mobility while adding passive protection against undesired back-bending.

C. Reconfigurability

The spine's modularity supports multiple layouts. In the tested configuration (Fig. 3b), self-locking modules are placed at the top and bottom, with four 2-DoF modules in between, rotated by 90° relative to each other. This arrangement balances stiffness with RoM, approximating human torso flexibility while remaining reconfigurable for task-specific demands. Alternative layouts could emphasize stability (by stacking more self-locking modules) or mobility (by including more 3-DoF units), highlighting the adaptability of the approach.

D. Actuation System

The system combines pneumatic and tendon-driven actuation (Fig. 3a,c,d). The inflatable shell anchors to the spine and, when inflated, exerts vertical tension that deploys the collapsed modules while enclosing them in a compliant outer layer intended to reduce snag and hard-contact exposure. Inflation also contributes to external stiffening and eliminates exposed rigid components.

Tendons route through pre-cut passageways and terminate in a servo control base. Six servo motors independently actuate tendon groups:

- **Servos 1–2:** anterior/posterior tendons (sagittal bending).
- **Servos 3–4:** lateral tendons (frontal bending).
- **Servos 5–6:** self-locking wings (engagement to lock and disengagement for collapse).

Pulling a tendon shortens its hinge and produces bending. For unidirectional hinges, tendons also unlock the passive constraint. This routing yields discrete, repeatable joint control while pneumatic inflation provides safe deployment and tunable stiffness.

The combined actuation strategy separates deployment from joint control. Alternative soft actuation methods such as pneumatic artificial muscle (PAM) or shape memory alloy (SMA) systems can generate contraction [39], but integrating them at each joint would couple actuation force and deformation directly to pressure or thermal dynamics [40]–[42]. In contrast, tendon-driven actuation allows independently addressable, bidirectional joint control while keeping motors centralized at the base [39], [43]. In this torso-scale architecture, pneumatic inflation regulates global deployement and stiffness of the shell, whereas tendons define and actuate discrete bending axes. This functional separation preserves controllable multi-DoF motion within

an inflatable encapsulation while limiting per-joint pneumatic routing complexity.

E. Design Rationale and Implications

The hybrid design leverages the complementary strengths of each element: the inflatable shell provides compact storage, safe deployment, and external stiffening; the origami spine localizes bending to discrete joints; and tendon actuation yields repeatable, joint-level control. Together, these features create a torso architecture that is reconfigurable, compliant, and controllable at humanoid scale.

The deployability ratio is a key feature: the torso folds down to roughly 12.5% of its deployed height, enabling efficient transport and storage. This makes the design relevant for field robotics, where compact packing and rapid deployment are critical. At the same time, hinge durability and tendon fatigue remain challenges for long-term use, suggesting directions for future refinement. Overall, the design demonstrates how origami principles, when combined with inflatable structures and tendon actuation, can yield a robust torso-scale mechanism that balances mobility, contact compliance, and compactness.

III. Experiments

We evaluated the torso's performance in range of motion (RoM), open-loop precision, and lateral stiffness, as well as the effect of inflation pressure on stiffness and RoM. Unless otherwise noted, tests were conducted at 70 kPa. This value was identified through preliminary pressure sweeps as the minimum pressure required to achieve full geometric deployment of all spine modules while maintaining stable shell tension. Below this threshold, incomplete extension and localized wrinkling were observed, leading to reduced structural stability and inconsistent motion. Higher pressures (80–120 kPa) were tested for trade-off analysis, while pressures above 120 kPa were avoided due to increasing shell strain and risk of seam damage.

A. Experimental Setup

The torso was fixed at its base and instrumented with visual markers placed at the upper rim for motion capture. Markers were tracked using a calibrated camera system (Sony Cyber-shot DSC-RX100). A wheeled digital force gauge (Mxmoonfree ZMF-50N, 0–50 N range) mounted on a linear rail applied controlled lateral loads (Fig. 4). The gauge resolution was 0.01 N, ensuring that small stiffness variations could be resolved. Six servo motors (FEETCH FB5311M-360) actuated tendon groups, housed in a 3D-printed base, and were commanded through open-loop signals. Inflation was supplied by an air compressor (Mastercraft 2-Gallon, model 058-9857-2).

Two actuation conditions were tested:

- **Pneumatic-only:** torso inflated to the target pressure, tendons inactive (no tension).
- **Combined actuation:** torso inflated, tendons engaged to contribute to stiffness (minimum tension).

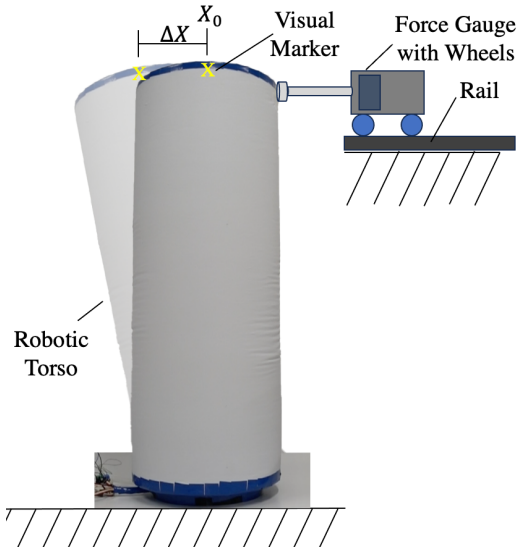

Fig. 4. Experimental setup with visual markers and wheeled force gauge on a rail; Δx measured at the top rim.

TABLE I
RoM Comparison Between Robotic Spine and Anatomical Standards (°)

	Left	Right	Back	Front
Spine	28.75	28.50	27.60	27.44
Anatomy	30	30	26	22

Each experiment was repeated across 10–15 trials per condition. Trials were separated by deflation and re-inflation to capture variability across deployments.

B. Range of Motion

The RoM was measured in both medial–lateral (M–L) and anteroposterior (A–P) planes. For each direction, the torso was actuated until motion slowed significantly, and endpoint angles were recorded across multiple trials. Results are summarized in Table I and illustrated in Fig. 5. Compared to anatomical standards [44], the robotic torso showed slightly reduced M–L RoM but exceeded natural A–P values, confirming that the origami-inflatable design affords mobility beyond human norms in sagittal motion.

C. Open-loop Precision

For each bending direction, the torso was deflated and reinflated between trials to assess repeatability. Endpoint distributions were characterized using 95% covariance ellipses (Table II). Results show deviations on the order of 35–66 mm in the major axis and 11–16 mm in the minor axis, reflecting variability due to re-inflation but consistent directional control. While absolute repeatability was moderate, the relative consistency of motion trajectories indicates that tendon-driven bending reliably localized motion along intended axes.

D. Lateral Stiffness

Lateral stiffness was measured by applying lateral force with the gauge until the torso's base lifted. Here, lateral

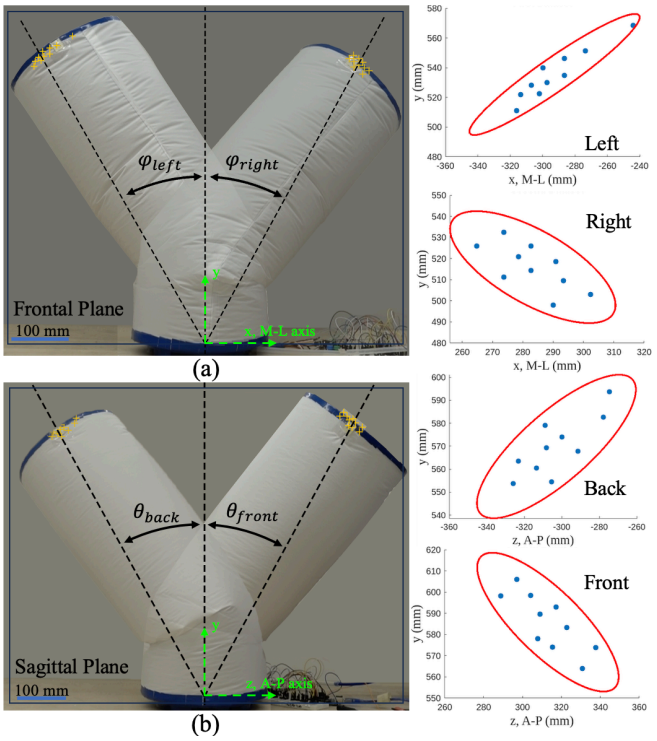

Fig. 5. Range of motion in (a) frontal and (b) sagittal planes. Scatter points show tip traces; ellipses indicate repeatability.

TABLE II
OPEN-LOOP PRECISION (MM) IN EACH DIRECTION

Direction	Semi-major axis	Semi-minor axis
Left	65.66	10.77
Right	34.86	15.22
Back	50.06	16.19
Front	46.28	15.84

stiffness refers to the slope of the force–displacement curve (N/mm), i.e., the incremental force required per unit lateral displacement. Force–displacement data were recorded under pneumatic-only and combined conditions (Fig. 6). Linear fits were used to extract stiffness values (Table III). Combined actuation approximately doubled stiffness relative to pneumatic-only inflation, demonstrating that tendons contributed effective joint stiffening rather than merely adding passive resistance.

E. Pressure Trade-offs

To study pressure effects, lateral stiffness was measured across 70–120 kPa at 10 kPa intervals, with tendons slack. Mean stiffness increased linearly with pressure, as shown in Fig. 7. In parallel, RoM was tested under fixed-stroke tendon actuation (1.5 s cycles). Higher pressures reduced displacement due to increased stiffness, confirming a tunable balance between stability and mobility. These results illustrate how the torso can be configured either for high compliance and flexibility at low pressures or for stability and load support at higher pressures.

TABLE III
LATERAL STIFFNESS (N/MM) IN M–L AND A–P DIRECTIONS

State	M–L	A–P
Combined actuation	0.0118	0.0117
Pneumatic-only	0.0059	0.0056

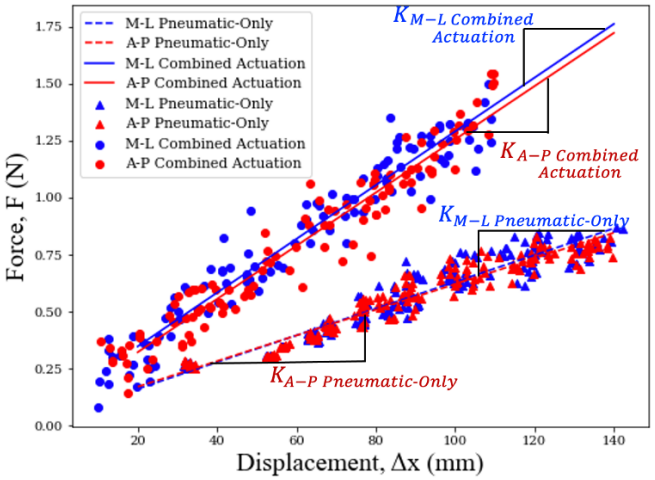

Fig. 6. Force–displacement data for M–L and A–P directions under pneumatic-only and combined actuation. Lines represent fitted stiffness.

IV. RESULTS AND DISCUSSION

A. Range of Motion and Precision

The torso achieved bending in both frontal (M–L) and sagittal (A–P) planes with repeatable trajectories (Fig. 5). Table I compares measured RoM against anatomical standards [44]. While M–L flexibility was slightly reduced, the A–P range exceeded human norms, showing that the design supports interaction-relevant compliance and mobility while allowing extended functionality.

Open-loop precision analysis (Table II) indicated moderate repeatability, with deviations on the order of 35–66 mm along the major axis and 11–16 mm along the minor axis. This variability corresponds to approximately 40–80% of a single module height (80 mm), indicating that deviations were on the order of one joint's displacement while overall motion trajectories remained aligned with the intended bending direction. Also, these variations arise primarily from re-inflation between trials, while the directional consistency of bending was preserved. For humanoid interaction, this suggests that the torso can reliably follow bending commands but would benefit from closed-loop feedback for high-accuracy tasks.

Expressed relative to the full deployed torso height of 480 mm, the observed repeatability deviations correspond to approximately 7–14% of overall height. This places the variability in the context of torso-scale motion, where such errors remain acceptable for gross posture changes but would be limiting for fine manipulation tasks. From a human–robot interaction standpoint, this suggests that the torso can reproducibly generate bending behaviors for interaction or assistance, while future integration of sensing and closed-

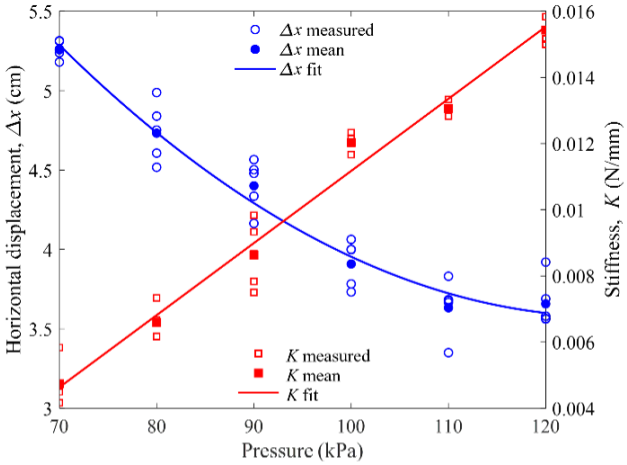

Fig. 7. Pressure trade-offs: stiffness increases with inflation pressure while RoM decreases under fixed-stroke actuation.

loop control will be required to achieve precise posture regulation.

Human trunk stabilization relies on task-dependent antagonistic muscle co-contraction, with neuromuscular control adjusting stiffness even under constant external loads [45], [46]. Such regulation introduces inherent variability in trunk motion, refelcting a balance between compliance and stability rather than strict positional precision. The moderate variability observed across deployments in the present system therefore reflects a comparable compliance-stability trade-off inherent to inflatable structures. Increased compliance reduces hard-contact severity at the cost of absolute positional precision. In practice, this allows the torso to remain compliant during contact-rich interaction, while avoiding brittle, high-stiffness behavior that can amplify peak impact forces during incidental bumps.

B. Lateral Stiffness Modulation

Force–displacement results demonstrated that tendon engagement increased stiffness (Fig. 6). Compared to pneumatic-only inflation, combined actuation approximately doubled stiffness (Table III). This shows that tendons provide active reinforcement of the origami joints.

For context, human trunk stiffness increases with muscle activation, as greater abdominal co-contraction produces higher resistance to external bending moments [45], [47]. Although the absolute stiffness values of the present system is lower due to its lightweight inflatable structure, the observed$\sim 2\times$ modulation reflects a comparable principle of adjustable stiffness. This tunability enables the torso to shift between compliant behavior for contact-rich interaction and increased structural support for posture stabilization or load-bearing tasks. At this system level, such modulation increases resistance to external perturbations and appendage-induced tipping moments, without sacrificing baseline compliance.

Tendon–pneumatic hybrids have previously been explored in manipulators at smaller scales [33], [34]. The present work demonstrates the effect of such hybrid actuation at the humanoid torso scale within an inflatable protective shell, highlighting integration at a system level rather than module or limb level.

C. Pressure–Performance Trade-offs

Experiments across 70–120 kPa showed a tunable balance between stiffness and mobility (Fig. 7). Stiffness increased nearly linearly with pressure, while RoM decreased under fixed-stroke tendon actuation. This tunability allows the system to be configured either for compliant interaction (lower pressures) or for stability and load support (higher pressures). Among these, humanoid torso safety is a particularly compelling application: the inflatable shell ensures compliant contact with humans, while adjustable stiffness allows the torso to shift between compliant interaction and stable support during posture regulation or load transfer.

The choice of 70 kPa as a baseline reflects the minimum inflation needed for full deployment without overstressing the shell, while tests were capped at 120 kPa to avoid damage. These bounds provide a safe and practical operating range.

The ability to modulate stiffness and RoM through inflation pressure is particularly relevant because lower pressures increase compliance, which is commonly used as a design strategy to reduce hard-contact severity during contact. At low pressures, the torso remains highly compliant, which can reduce hard-contact severity during incidental bumps. At higher pressures, the torso can provide more stable support, enabling load-bearing or posture-maintaining functions. This tunability makes the system adaptable to varied contexts, from contact-rich interaction to stable operation in unstructured environments.

D. Comparison to Existing Approaches

Direct quantitative comparisons are difficult because few torso-scale devices have been reported in the literature. To provide context, Table IV summarizes representative prior approaches at the module, limb, and inflatable joint level, highlighting the relative system-level trade-offs in deployability, safety, and stiffness. Here, stiffness is used in a *relative, system-level* sense to describe whether prior approaches provide mechanisms for adjusting structural resistance to lateral displacement. This is distinct from the quantitative stiffness values (N/mm) reported in Table III; the table conveys whether stiffness is tunable, fixed, or based solely on internal pressure. Tendon-driven devices such as the Exo-Glove [28] achieve precise motion through cables but are not designed for deployability or torso-scale integration. Inflatable structures such as Niiyama et al.'s blower-powered joint [27] demonstrate compactness and safe human-scale interaction, but stiffness adjustment beyond pressure variation was not reported. Origami-inspired manipulators [20], [21] illustrate folding-based motion and stiffness strategies at the module level, but have not been applied to torso-scale humanoid systems.

In contrast, this work combines compact self-deployment (folds to 12.5% of deployed height), discrete bending axes defined by origami hinges, and adjustable stiffness, with

TABLE IV

REPRESENTATIVE APPROACHES FOR HUMANOID-SCALE OR RELATED SPINES

Approach	Deploy/Safety	Stiffness (relative)
Exo-Glove (tendon-driven) [28]	No / No	High (fixed)
Inflatable joint (blower-powered) [27]	Yes / Yes	Pressure-based
Origami modules (pneumagami) [20]	Partial / Partial	Moderate (module-level)
Origami arm (self-locking) [21]	Partial / No	Locking (module-level)
This work	**Yes (12.5%) / Yes**	**Adjustable ($\approx$2$\times$)**

tendon engagement approximately doubling stiffness relative to pneumatic-only operation.

E. System-Level Stability Considerations

The present study evaluates the torso as a modular subsystem rather than a complete humanoid structure. In a full robot, global stability depends on center-of-mass (CoM) location, support polygon geometry, and lower-body control. While the torso alone does not determine tipping, its its bending compliance affects how external loads or appendage motions shift the effective CoM. In the current prototype, most actuation hardware is located at the bottom of the torso, resulting in a relatively low mass distribution and passive tipping tendencies during testing. When integrated with arms or manipulators, tendon engagement and elevated inflation pressures can raise structural stiffness, reducing lateral deflection under external moments and limiting CoM displacement. This enables a mode-switching strategy: compliant operation for contact-rich interaction and higher-stiffness configurations for posture stabilization and load-bearing. Full falling prevention ultimately requires coordinated lower-limb or mobile-base control. However, the demonstrated stiffness modulation provides a mechanical foundation for stable integration with appendages.

F. Implications and Future Directions

The results highlight the benefits of combining origami-inspired skeletal modules with an inflatable shell. The torso can be collapsed to 12.5% of its deployed height for portability and rapid deployment. Tendon engagement approximately doubled stiffness, and pneumatic pressure tuning allowed continuous adjustment of performance.

For use in humanoid robots, improvements are needed in hinge durability, tendon fatigue resistance, and consistency across deployments. Closed-loop control using embedded sensing (e.g., IMUs, pressure sensors) could enhance precision. Beyond humanoids, the deployable architecture may be applicable in field robotics, wearable assistive devices, and other systems requiring compactness, safety, and stiffness modulation. Inflation and deflation cycle times were not characterized in this study but remain an important factor for assessing deployability in time-critical applications.

V. CONCLUSION

This work presented a deployable inflatable robotic torso that integrates an origami-inspired spine with pneumatic and tendon-driven actuation. The inflatable shell enables compact storage, self-deployment, and external stiffening, while the origami spine defines discrete bending axes and tendon actuation provides repeatable control. Experiments showed that the torso achieves human-comparable range of motion, with flexion/extension exceeding anatomical values, and demonstrated moderate repeatability across deployments, consistent with the compliance-precision trade-offs discussed. Stiffness was shown to be adjustable, with tendon engagement approximately doubling lateral stiffness relative to pneumatic-only inflation, and pressure variation providing a continuous trade-off between mobility and stability. These findings indicate that the origami-inflatable architecture provides tunable mechanical compliance and stiffness modulation at torso scale, which are key prerequisites for safer physical interaction. While direct human-robot interaction experiments were beyond the scope of this study, the demonstrated pressure-dependent stiffness and compliant shell design establish the mechanical basis for future safety validation. Future work will address hinge durability, tendon fatigue resistance, and the integration of closed-loop control using embedded sensing (e.g., IMUs, pressure sensors). In parallel, comparative testing with human surrogates will be used to quantify contact forces and pressures during representative interactions, and inflation/deflation cycle times will be measured to evaluate deployment readiness. Together, these steps will establish the practicality of the system for integration into humanoid robots and other deployable platforms.

ACKNOWLEDGMENT

The authors used AI-based language editing tools solely for grammar checking and minor sentence-level polishing. All technical content, analysis, and scientific claims were written and verified by the authors.

REFERENCES

[1] T. Ranzani, M. Cianchetti, G. Gerboni, I. D. Falco, and A. Menciassi, "A soft modular manipulator for minimally invasive surgery: Design and characterization of a single module," *IEEE Transactions on Robotics*, vol. 32, no. 1, pp. 187–200, Feb. 2016.

[2] C. Cy and P. Rm, "Soft robotic devices for hand rehabilitation and assistance: a narrative review," *Journal of Neuroengineering and Rehabilitation*, vol. 15, no. 1, Feb. 2018.

[3] Y. Zhou and H. Li, "A scientometric review of soft robotics: Intellectual structures and emerging trends analysis (2010–2021)," *Frontiers in Robotics and AI*, vol. 9, 2022.

[4] M. Cianchetti, C. Laschi, A. Menciassi, and P. Dario, "Biomedical applications of soft robotics," *Nature Reviews Materials*, vol. 3, no. 6, pp. 143–153, Jun. 2018.

[5] A. Elor, S. Lessard, M. Teodorescu, and S. Kurniawan, "Project Butterfly: Synergizing immersive virtual reality with actuated soft exosuit for upper-extremity rehabilitation," in *2019 IEEE Conference on Virtual Reality and 3D User Interfaces (VR)*, Mar. 2019, pp. 1448–1456.

[6] A. S. Ciullo, J. M. Veerbeek, E. Temperli, A. R. Luft, F. J. Tonis, C. J. W. Haarman, A. Ajoudani, M. G. Catalano, J. P. O. Held, and A. Bicchi, "A novel soft robotic supernumerary hand for severely affected stroke patients," *IEEE Transactions on Neural Systems and Rehabilitation Engineering*, vol. 28, no. 5, pp. 1168–1177, May 2020.

[7] L. Sy, T. T. Hoang, M. Bussu, M. T. Thai, P. T. Phan, H. Low, D. Tsai, M. A. Brodie, N. H. Lovell, and T. N. Do, "M-SAM: Miniature and soft artificial muscle-driven wearable robotic fabric exosuit for upper limb augmentation," in *2021 IEEE 4th International Conference on Soft Robotics (RoboSoft)*, Apr. 2021, pp. 575–578.

[8] S. Pattinson, M. Huber, S. Kim, J. Lee, S. Grunsfeld, R. Roberts, G. Dreifus, C. Meier, L. Liu, N. Hogan, and A. J. Hart, "Additive manufacturing of biomechanically tailored meshes for compliant wearable and implantable devices," *Advanced Functional Materials*, vol. 29, Jun. 2019.

[9] T. Amadeo, D. Van Lewen, T. Janke, T. Ranzani, A. Devaiah, U. Upadhyay, and S. Russo, "Soft robotic deployable origami actuators for neurosurgical brain retraction," *Frontiers in Robotics and AI*, vol. 8, 2022.

[10] I. Ario, M. Nakazawa, Y. Tanaka, I. Tanikura, and S. Ono, "Development of a prototype deployable bridge based on origami skill," *ISARC Proceedings*, pp. 981–986, Jun. 2011.

[11] Z. Ding, C. Wang, H. Wu, and X. Liu, "Dynamic analysis of modular space deployable supportingstructure," in *2018 10th International Conference on Measuring Technology and Mechatronics Automation (ICMTMA)*, Feb. 2018, pp. 337–340.

[12] A. Zhu, H. Shen, Z. Shen, J. Song, and Y. Tu, "Innovative design for portability of unpowered military load exoskeleton robot," in *2018 IEEE International Conference on Information and Automation (ICIA)*, Aug. 2018, pp. 744–749.

[13] M. Dziekan, S. Jubaer, V. Sell, S. Manda, A. Aboelzahab, S. Romero-Velasteguí, J. C. Mejía-Viana, and J. A. Uquillas, "Design of a low-cost, portable, and automated cardiopulmonary resuscitation device for emergency scenarios in Ecuador," in *2017 IEEE Second Ecuador Technical Chapters Meeting (ETCM)*, Oct. 2017, pp. 1–6.

[14] F. Fuentes and L. H. Blumenschein, "Deployable robotic structures via passive rigidity on a soft, growing robot," in *2023 IEEE International Conference on Soft Robotics (RoboSoft)*, Apr. 2023, pp. 1–7.

[15] P. Palmieri, M. Gaidano, M. Troise, L. Salamina, A. Ruggeri, and S. Mauro, "A deployable and inflatable robotic arm concept for aerospace applications," in *2021 IEEE 8th International Workshop on Metrology for AeroSpace (MetroAeroSpace)*, Jun. 2021, pp. 453–458.

[16] A. Alspach, J. Kim, and K. Yamane, "Design and fabrication of a soft robotic hand and arm system," in *2018 IEEE International Conference on Soft Robotics (RoboSoft)*, Apr. 2018, pp. 369–375.

[17] M. Hofer, J. Zughaibi, and R. D'Andrea, "Design and control of an inflatable spherical robotic arm for pick and place applications," *Actuators*, vol. 10, no. 11, p. 299, Nov. 2021.

[18] J. M. Bern, F. Zargarbashi, A. Zhang, J. Hughes, and D. Rus, "Simulation and fabrication of soft robots with embedded skeletons," in *2022 International Conference on Robotics and Automation (ICRA)*, May 2022, pp. 5205–5211.

[19] Y. Liao and S. Krishnan, "Deployable scissor structures: Classification of modifications and applications," *Automation in Construction*, vol. 165, p. 105547, Sep. 2024.

[20] M. A. Robertson, O. C. Kara, and J. Paik, "Soft pneumatic actuator-driven origami-inspired modular robotic "pneumagami"," *The International Journal of Robotics Research*, vol. 40, no. 1, pp. 72–85, Jan. 2021.

[21] K. Sj, L. Dy, J. Gp, and C. Kj, "An origami-inspired, self-locking robotic arm that can be folded flat," *Science Robotics*, vol. 3, no. 16, Mar. 2018.

[22] Q. Ze, S. Wu, J. Dai, S. Leanza, G. Ikeda, P. C. Yang, G. Iaccarino, and R. R. Zhao, "Spinning-enabled wireless amphibious origami millirobot," *Nature Communications*, vol. 13, no. 1, p. 3118, Jun. 2022.

[23] A. R. Deshpande, Z. T. Ho Tse, and H. Ren, "Origami-inspired bi-directional soft pneumatic actuator with integrated variable stiffness mechanism," in *2017 18th International Conference on Advanced Robotics (ICAR)*, Jul. 2017, pp. 417–421.

[24] S. S. Kwak, S. Park, D. Kang, H. Lee, J. H. Yang, Y. Lim, and K. Song, "PopupBot: A robotic pop-up space for children: Origami-based transformable robotic playhouse recognizing children's intention," in *2022 17th ACM/IEEE International Conference on Human-Robot Interaction (HRI)*, Mar. 2022, pp. 1196–1197.

[25] J. Fathi, T. J. Oude Vrielink, M. S. Runciman, and G. P. Mylonas, "A deployable soft robotic arm with stiffness modulation for assistive living applications," in *2019 International Conference on Robotics and Automation (ICRA)*, May 2019, pp. 1479–1485.

[26] N. S. Usevitch, Z. M. Hammond, M. Schwager, A. M. Okamura, E. W. Hawkes, and S. Follmer, "An untethered isoperimetric soft robot," *Science Robotics*, vol. 5, no. 40, p. eaaz0492, Mar. 2020.

[27] R. Niiyama, Y. ah Seong, Y. Kawahara, and Y. Kuniyoshi, "Blower-powered soft inflatable joints for physical human-robot interaction," *Frontiers in Robotics and AI*, vol. 8, 2021.

[28] H. In, B. B. Kang, M. Sin, and K.-J. Cho, "Exo-glove: A wearable robot for the hand with a soft tendon routing system," *IEEE Robotics & Automation Magazine*, vol. 22, no. 1, pp. 97–105, Mar. 2015.

[29] W. R. Wockenfuß, V. Brandt, L. Weisheit, and W.-G. Drossel, "Design, modeling and validation of a tendon-driven soft continuum robot for planar motion based on variable stiffness structures," *IEEE Robotics and Automation Letters*, vol. 7, no. 2, pp. 3985–3991, Apr. 2022.

[30] N. Saga, J. Nagase, and T. Saikawa, "Development of a tendon driven system using a pneumatic balloon," in *IEEE International Conference Mechatronics and Automation, 2005*, vol. 2, Jul. 2005, pp. 1087–1092 Vol. 2.

[31] D. Rus and M. T. Tolley, "Design, fabrication and control of soft robots," *Nature*, vol. 521, no. 7553, pp. 467–475, May 2015.

[32] M. Park, W. Kim, S.-Y. Yu, J. Cho, W. Kang, J. Byun, U. Jeong, and K.-J. Cho, "Deployable soft origami modular robotic arm with variable stiffness using facet buckling," *IEEE Robotics and Automation Letters*, vol. 8, no. 2, pp. 864–871, Feb. 2023.

[33] Z. Zhang, S. Tang, W. Fan, Y. Xun, H. Wang, and G. Chen, "Design and analysis of hybrid-driven origami continuum robots with extensible and stiffness-tunable sections," *Mechanism and Machine Theory*, vol. 169, p. 104607, Mar. 2022.

[34] Z. Zhang, G. Chen, H. Wu, L. Kong, and H. Wang, "A pneumatic/cable-driven hybrid linear actuator with combined structure of origami chambers and deployable mechanism," *IEEE Robotics and Automation Letters*, vol. 5, no. 2, pp. 3564–3571, Apr. 2020.

[35] C. C. Johnson, A. Clawson, and M. D. Killpack, "Baloo: A Large-Scale Hybrid Soft Robotic Torso for Whole-Arm Manipulation," Mar. 2025.

[36] H. Liu, Y. Yang, T. Wang, J. Yin, and H. Wang, "Bioinspired growable humanoid robot with bone-mimetic linkages for versatile mobility," *Science Advances*, vol. 12, no. 4, p. eaea2831, Jan. 2026.

[37] S. Lin, H. Liu, C. Wu, L. Huang, and Y. Chen, "Anti-falling of wheeled humanoid robots based on a novel variable stiffness mechanism," *Smart Materials and Structures*, vol. 34, no. 8, p. 085002, Aug. 2025.

[38] T. Sugiyama, K. Kutsuzawa, D. Owaki, and M. Hayashibe, "Individual deformability compensation of soft hydraulic actuators through iterative learning-based neural network," *Bioinspiration & Biomimetics*, vol. 16, no. 5, p. 056016, Nov. 2021.

[39] M. Li, A. Pal, A. Aghakhani, A. Pena-Francesch, and M. Sitti, "Soft actuators for real-world applications," *Nature reviews. Materials*, vol. 7, pp. 235–249, Mar. 2022.

[40] A. Zhagiparova, V. Golubev, and D. Kim, "Recent Developments in Pneumatic Artificial Muscle Actuators," *Actuators*, vol. 14, no. 12, Nov. 2025.

[41] Z. Shami, T. Arslan, and P. Lomax, "Wearable Soft Robots: Case Study of Using Shape Memory Alloys in Rehabilitation," *Bioengineering*, vol. 12, no. 3, p. 276, Mar. 2025.

[42] E. Shi, X. Zhong, T. Wang, X. Li, C. Bu, and X. Zhao, "Adaptive control for shape memory alloy actuated systems with applications to human–robot interaction," *Frontiers in Neuroscience*, vol. 18, Jan. 2024.

[43] N. Sholl and K. Mohseni, "High-stretch, tendon-driven, fiber-reinforced membrane soft actuators with multiple active degrees of freedom," *Communications Engineering*, vol. 3, no. 1, p. 25, Feb. 2024.

[44] Janis Savlovskis, "Range of motion (ROM) of the cervical, thoracic and lumbar spine in the traditional anatomical planes."

[45] K. P. Granata and K. F. Orishimo, "Response of trunk muscle coactivation to changes in spinal stability," *Journal of Biomechanics*, vol. 34, no. 9, pp. 1117–1123, Sep. 2001.

[46] P. W. Hodges and C. A. Richardson, "Contraction of the abdominal muscles associated with movement of the lower limb," *Physical Therapy*, vol. 77, no. 2, pp. 132–142; discussion 142–144, Feb. 1997.

[47] S. H. M. Brown and S. M. McGill, "How the inherent stiffness of the in vivo human trunk varies with changing magnitudes of muscular activation," *Clinical Biomechanics*, vol. 23, no. 1, pp. 15–22, Jan. 2008.